ARTICLE IN PRESS
JID: JMAA [m5+;December 10, 2021;21:8]

Available online at www.sciencedirect.com

ScienceDirect

Journal of Magnesium and Alloys xxx (xxxx) xxx

www.elsevier.com/locate/jma

Full Length Article

Activation of <c> dislocations in Mg with solute Y

Alireza Maldar[a], Leyun Wang[a,*], Boyu Liu[b], Wenjun Liu[c], Zhaohui Jin[d], Bijin Zhou[a,e], Xiaoqin Zeng[a]

[a] National Engineering Research Center of Light Alloy Net Forming, Shanghai Jiao Tong University, Shanghai 200240, China
[b] State Key Laboratory for Mechanical Behavior of Materials, Xi'an Jiaotong University, Xi'an 710049, China
[c] Advanced Photon Source, Argonne National Laboratory, IL 60439, USA
[d] Shenyang National Laboratory for Materials Science, Institute of Metal Research, Chinese Academy of Sciences, 72 Wenhua Road, Shenyang 110016, China
[e] School of Mechanical Engineering, Suzhou University of Science and Technology, Suzhou 215009, China

Received 3 September 2021; received in revised form 2 November 2021; accepted 7 November 2021
Available online xxx

Abstract

Mg-Y cast alloy shows excellent ductility (elongation to failure > 15%) compared with pure Mg and commercial Mg cast alloys. By monitoring the microstructure evolution during an *in situ* tensile test of a Mg-2.5 wt%Y alloy, we identify the activation of prismatic <c> slip, which is rare in Mg. Synchrotron X-ray micro-beam Laue diffraction (μ-Laue) and transmission electron microscopy revealed the morphology of prismatic <c> slip bands and individual <c> dislocations. Density functional theory and molecular dynamics calculations indicate that solute Y can significantly reduce the stacking fault energy (SFE) along <c> direction on prismatic plane in Mg lattice and thus facilitate the nucleation of <c> dislocations during deformation. The presence of free <c> dislocations in the Mg lattice can also lead to nucleation of {10–12} twins even under unfavorable geometric conditions.

1. Introduction

Magnesium is the lightest structural material with very high specific strength (*i.e.* strength-to-weight ratio), making it attractive for automobile and aerospace applications. Currently, the usage of Mg is largely limited by its ductility and formability at room temperature. As a hexagonal metal, deformation of Mg is predominantly accommodated by basal slip $\{0001\}\langle 1\bar{2}10\rangle$ and tensile twinning $\{10\bar{1}2\} < \bar{1}011 >$ [1,2], while non-basal slip such as prismatic slip $\{10\bar{1}0\}\langle 1\bar{2}10\rangle$ and pyramidal II <c+a> slip $\{11\bar{2}2\}\langle \bar{1}\bar{1}23\rangle$ are much more difficult to be activated unless under extremely favorable geometric conditions, for instance under uniaxial tension parallel with the {0001} plane or under uniaxial compression along the <0001> direction (*i.e.* c-axis) of single grains [3,4,5,6]. For pure Mg, it is estimated that the critical resolved shear stress (CRSS) of basal slip is one or two orders of magnitude lower than that of non-basal slip [7]. The general lack of ways to accommodate plastic deformation along the <c> direction limits Mg's ductility [8].

In the past decade, it has been found that selective rare earth alloying elements can significantly improve Mg's mechanical properties, especially its ductility [9,10,11,12, 13,14]. Microscopically, those rare earth elements have two major effects: (1) weakening the wrought texture of Mg, and (2) lowering the energy barrier for non-basal slip to be activated in Mg lattice. The latter is an intrinsic effect that will improve the ductility of both wrought and cast alloys. Influence of rare earth solutes on <c+a> slip and non-basal <a> slip has been extensively studied in recent years. It has been experimentally found that Y can enhance the activity of <c+a> dislocations in Mg [9]. Whether this is owing to solute atoms altering the I_1 stacking fault energy (SFE) on the basal plane, or their directly reducing the Peierls stress of <c+a> dislo-

* Corresponding author.
E-mail address: leyunwang@sjtu.edu.cn (L. Wang).

https://doi.org/10.1016/j.jma.2021.11.004

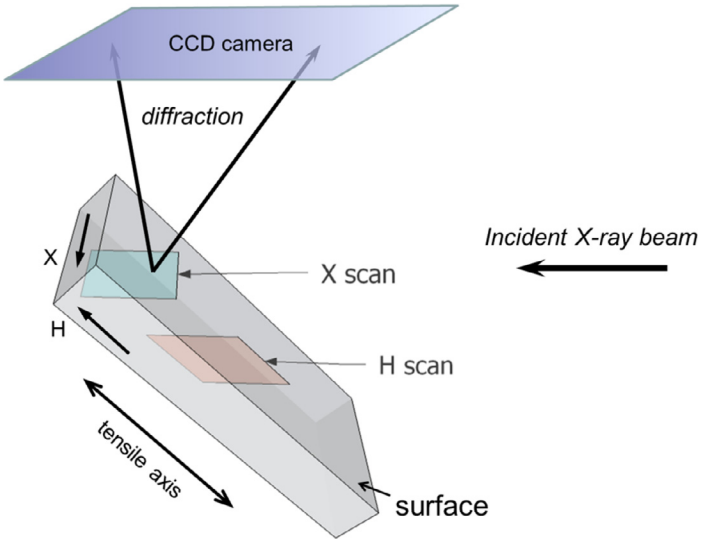

Fig. 1. **Geometry of μ-Laue line scans.** The specimen was 45° from the incident X-ray beam. Laue diffraction patterns were recorded on a CCD camera above the specimen. "X" and "H" directions describe the direction of motion of the specimen with respect to the stationary beam. The "H" direction is parallel to the tensile axis of the specimen.

cations on the pyramidal plane is still under debate according to different computational studies [15,16,17, 18]. By simulating the interaction of Y atoms with <a> dislocation cores, some authors suggested that Y can lower the energy barrier for <a> dislocation to cross slip from {0001} basal plane to $\{10\bar{1}0\}$ prismatic planes, thus promoting prismatic <a> slip [19,20]. Recent experimental studies of the deformation of Mg-Y using *in situ* three dimensional X-ray diffraction (3DXRD) and transmission electron microscopy indicated that the ratio of $CRSS_{prism}/CRSS_{basal}$ can be as low as 1.4∼2.7 [21,22], which further support the above theoretical predictions. In addition to enhancing non-basal dislocation activities, Y is known to suppress the nucleation of $\{10\bar{1}2\}$ twins in Mg [12,22]. In a Mg-10 wt.%Y alloy, activation of the uncommon $\{11\bar{2}1\}\langle\bar{1}\bar{1}26\rangle$ twin mode was identified [23]. This finding was attributed to Y obstructing the atomic shuffling process that is necessary for $\{10\bar{1}2\}$ twinning, while it has less impact on $\{11\bar{2}1\}$ twinning that does not require atomic shuffling.

Compared with <a> and <c+a> dislocations, <c> dislocation with a [0001] Burgers vector has been long regarded as too energetically unstable to self-nucleate in Mg lattice during deformation. Fan et al. [24] computed the core structure of edge <c> dislocations in Mg using density function theory (DFT). The unstable stacking fault energy (USFE) associated with <c> slip was found to be ∼0.8 J/mm^2, which is significantly higher than that for pyramidal <c+a> slip (∼0.5 J/mm^2) [25]. The only occasions for <c> dislocations to form are either through local decomposition of <c+a> dislocations into <c> and <a> components [26,27,28,29], or through irradiation that creates many point defects in the Mg lattice [30]. In all those cases, <c> dislocations were assumed to form locally and be immobile. In the present paper, we report a long-range activity of <c> dislocations in a Mg-2.5 wt%Y cast alloy. The material shows an elongation to failure of more than 15%. Formation of prismatic slip bands were observed in a specimen during an *in situ* tensile experiment using electron backscatter diffraction (EBSD) based slip trace analysis [31].Synchrotron X-ray micro-beam Laue diffraction (μ-Laue) [32,33] and transmission electron microscopy (TEM) with focused ion beam (FIB) sample preparation further confirmed that those slip bands originated from <c> dislocations gliding on the $\{10\bar{1}0\}$ prismatic plane. DFT and molecular dynamics (MD) calculations were performed to elucidate the effect of Y solutes on the activity of <c> dislocations in Mg lattice.

2. Material and methods

2.1. *Specimen preparation and* in situ *tensile test.*

A binary Mg-2.5 wt.%Y alloy was prepared by casting. To achieve a homogeneous composition distribution, the melt was taken to 700 °C for 10 min before casting. Flat dog-bone tensile specimens with a gauge dimension of 18 mm (L) × 3.4 mm (W) × 1.4 mm (T) were prepared by electrical discharge machining (EDM). For the *in situ* tensile test, additional specimens with a gauge dimension of 5 mm (L) × 2 mm (W) × 1 mm (T) were extracted. They were grinded to a thickness of ∼0.7 mm and polished for EBSD measurements using a FEI Nanolab 200 scanning electron microscope (SEM). The EBSD data was analyzed using TSL/EDAX OIM^{TM} Analysis Software. During the *in situ* tensile test, the specimen was deformed by a MICROTEST 200 N (Deben, UK Limited) module with a nominal strain rate of 6.67 × 10^{-4} s^{-1}. The microstructure evolution close to the gauge center was monitored using an Olympus SZX10 optical microscope connected with a video recording system.

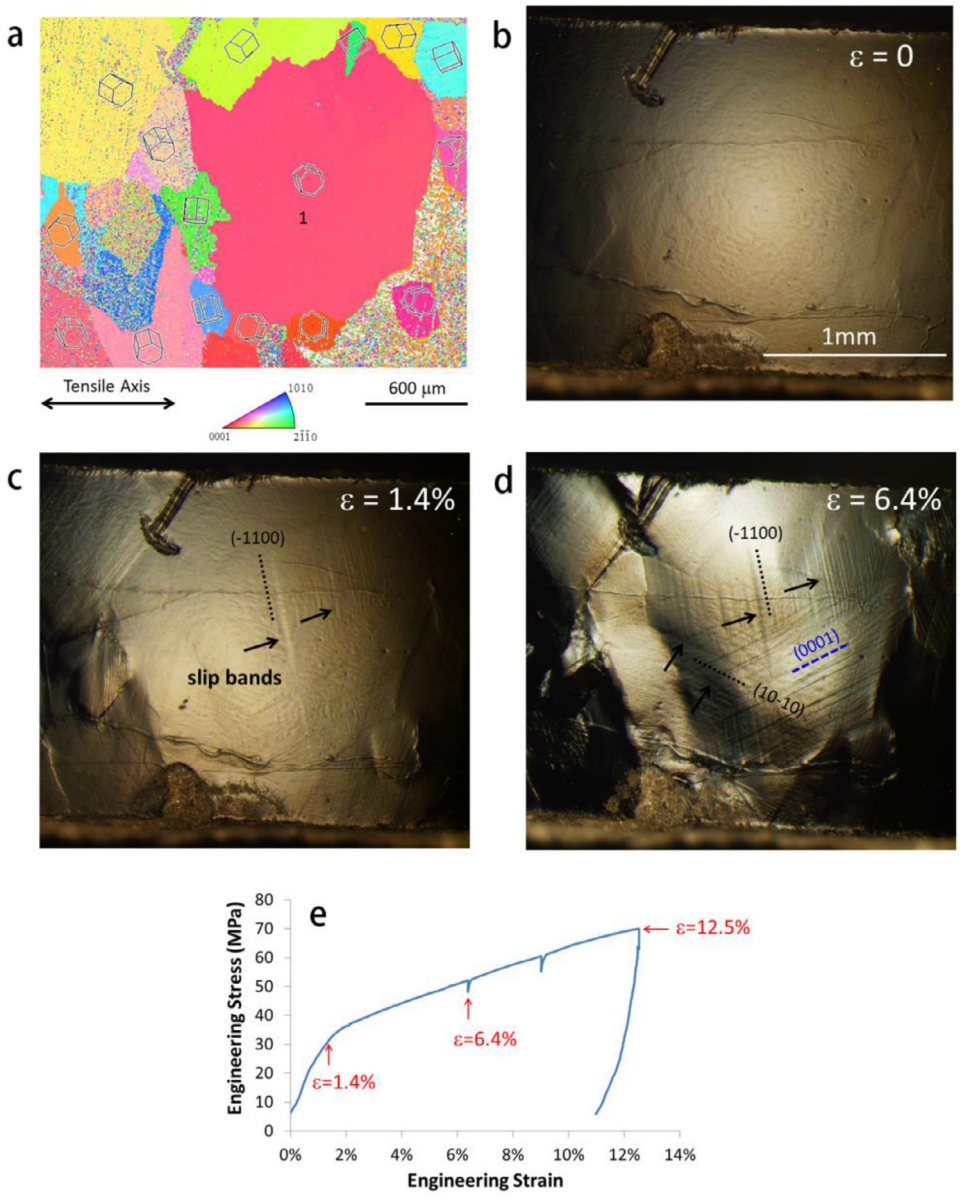

Fig. 2. **Microstructure evolution during the *in situ* tensile test.** (**a, b**) EBSD and optical micrograph of the same region at the gauge center of the specimen before deformation. (**c**) Optical micrograph taken at ε=1.4%. Slip bands parallel to the ($\bar{1}$100) prismatic plane were observed in Grain 1. (**d**) Optical micrograph taken at ε=6.4%. More slip activities developed in Grain 1. (**e**) Engineering stress-strain curve of the specimen.

2.2. Synchrotron X-ray micro-beam Laue diffraction (μ-Laue)

The μ-Laue experiment was performed at Beamline 34-ID-E at the Advanced Photon Source (APS) in Argonne National Laboratory in USA. A polychromatic micro-beam with the energy range of 8 − 25 keV and beam size of 0.5μm × 0.5μm was used to probe the specimen mounted at a 45° angle from the beam direction. Laue diffraction from all volumes along the beam path was recorded on a two-dimensional CCD camera above the specimen. A moving Pt edge served as the "differential aperture" to deconvolute Laue diffraction patterns of individual volume elements (*i.e.* voxels). By indexing each deconvoluted Laue pattern using the "LaueGo" program available at the beamline, crystallographic orientation of each voxel can be determined. When the beam scanned across the specimen surface along either the "H" direction (*i.e.* H scan) or the "X" direction (*i.e.* X scan), a subsurface orientation map can be generated, as depicted in Fig. 1.

2.3. TEM sample preparation and dislocation analysis

A thin lamella sample taken from one of the prismatic slip bands in Grain 1 (the grain is shown in Fig. 2) was prepared by FIB-milling and subsequent lift-out using a micromanipulator inside a FEI NanoLab DualBeam system. The lamella

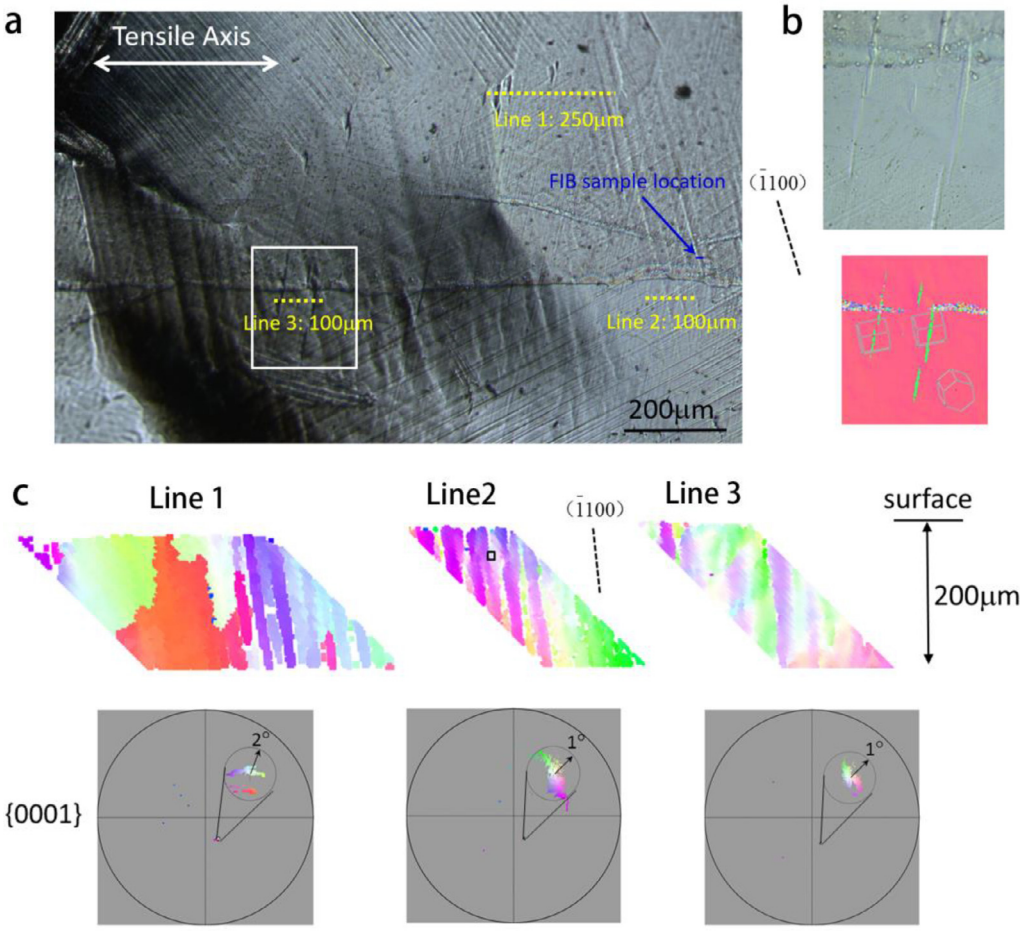

Fig. 3. **Further characterization of the post-deformation microstructure in Grain 1.** (**a**) Optical micrograph showing the upper part of Grain 1, where many ($\bar{1}100$) prismatic slip bands are present. The trace of the ($\bar{1}100$) prismatic plane is marked by a black dashed line. (**b**) Higher magnification image and associated EBSD orientation map showing small-sized twins of the $\{10\bar{1}2\}$ type. (**c**) Results of three μ-Laue line scans. The subsurface orientation maps are colored based on the orientation deviation of individual voxels from the average orientation. Straight slip bands extended underneath the surface. From plane trace analysis, they are parallel to the ($\bar{1}100$) prismatic plane.

Table 1
Average tensile properties of the Mg-2.5 wt.%Y alloy. YS: yield strength; UTS: ultimate tensile strength; ε_f: elongation to failure.

	YS (MPa)	UTS (MPa)	ε_f
Mg-2.5wt%Y	27	85	15.5%

was then transferred to small mesh grids and analyzed using a JEOL 2100F TEM. The lamella was tilted to the $[\bar{1}100]$ zone axis. Dark field (DF) images were taken at different diffraction vectors (**g**) under the two-beam condition. **g**·**b** analyses (**b** is the Burgers vector) were performed to determine the Burgers vector of dislocations [29,34].

3. Results

3.1. Tensile properties and in situ tensile test

Table 1 shows the average tensile properties of the Mg-2.5 wt.%Y cast alloy. Compared to pure Mg, this Mg-2.5 wt%Y alloy shows a significantly higher ε_f of 15.5%. To understand the underlying reason, we further investigated its deformation mechanisms through *in situ* characterization.

An *in situ* tensile specimen of the Mg-2.5 wt%Y cast alloy was loaded using a MICROTEST 200 N (Deben, UK) module under the optical microscope to record the microstructure evolution on the surface. Fig. 2 shows the initial grain geometry of the investigated area, development of slip bands during deformation, and the engineering stress-strain curve of this specimen. The material shows a large grain size with random grain orientation (Fig. 2a and b), a typical feature of Mg cast alloys. After a tensile strain of ~1.4%, slip bands developed in different grains. In particular, long slip bands that are about 70° away from the tensile axis appeared in Grain 1 (Fig. 2c). From EBSD-based slip trace analysis, those slip bands are parallel to the ($\bar{1}100$) prismatic plane of Grain 1 (Euler angles = (126°, 23°, 10°)). When the tensile strain reached 6.4%, more slip bands of this type developed in Grain 1 (Fig. 2d). In addition, slip bands parallel to the basal plane and slip bands parallel to another prismatic plane $(10\bar{1}0)$ also developed in the same grain. The specimen was unloaded after 12.5% strain without any sign of failure. From the

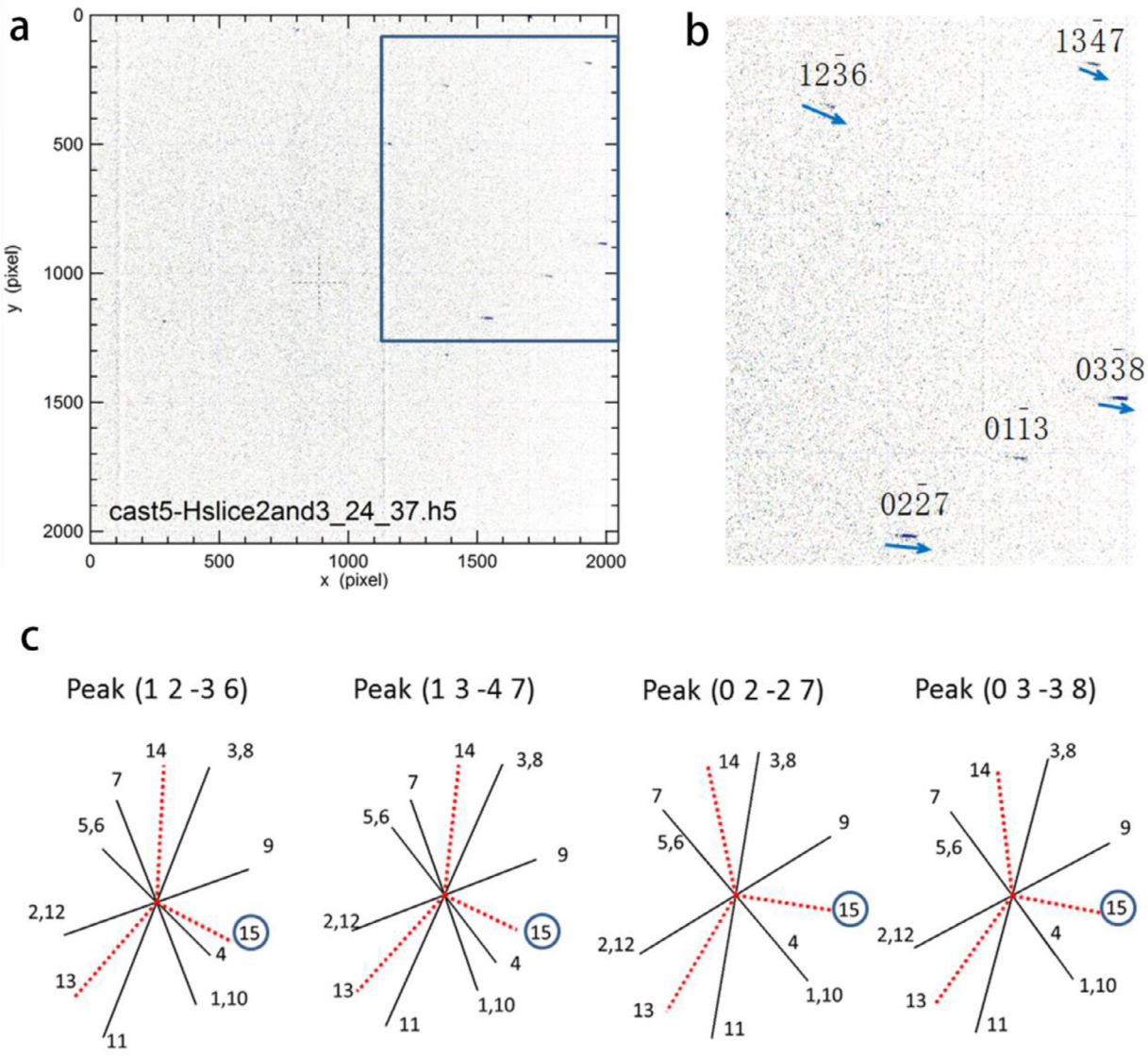

Fig. 4. **Diffraction peak streak analysis for identifying local GNDs.** (**a**) Deconvoluted Laue diffraction pattern for a voxel in line scan 2 marked in Fig. 3(c). The blue box region contains most of the visible peaks, so it is magnified and shown in (**b**) with indexed diffraction peaks. (**c**) Calculated streak direction for four peaks, assuming edge type GNDs from 15 individual slip systems. Slip system $(\bar{1}100)[0001]$ (#15) provides the best match between the calculated and observed peak streak direction (see blue arrows in (**b**)).

stress-strain curve in Fig. 2e, this specimen showed steady strain hardening in the plastic stage.

Fig. 3a shows a post-deformation optical micrograph of the upper part of Grain 1 with many $(\bar{1}100)$ prismatic slip bands. Small-sized $\{10\bar{1}2\}$ twins were observed in the vicinity of some slip bands, for example in the white box region which is magnified in Fig. 3b. Notably, the c-axis of Grain 1 was far away from the tensile direction, making it unfavorable for $\{10\bar{1}2\}$ twin nucleation. The Schmid factor (based on a global tensile stress) for the activated twin system is a negative value of −0.43. Thus, nucleation of these twins cannot be interpreted using the classic theory of twinning dislocations. Their formation was related to the <c> dislocations, as will be discussed later.

3.2. μ-Laue characterization of the prismatic slip bands

In order to further understand the prismatic slip bands in Grain 1, the specimen was taken to the Advanced Photon Source for μ-Laue characterization. Line scans were performed in three locations of Grain 1, as indicated in Fig. 3a. The step of each line scan was set to be 2 μm. The three line scans were all H scans, so the resultant orientation maps are of parallelogram shapes. Fig. 3c shows subsurface orientation maps from these line scans, all of which were solely inside Grain 1. Local orientation deviation up to 2° developed as a result of plastic deformation. Voxels in the orientation maps are colored based on the orientation deviation from the average value, as shown in the {0001} pole figures below. All

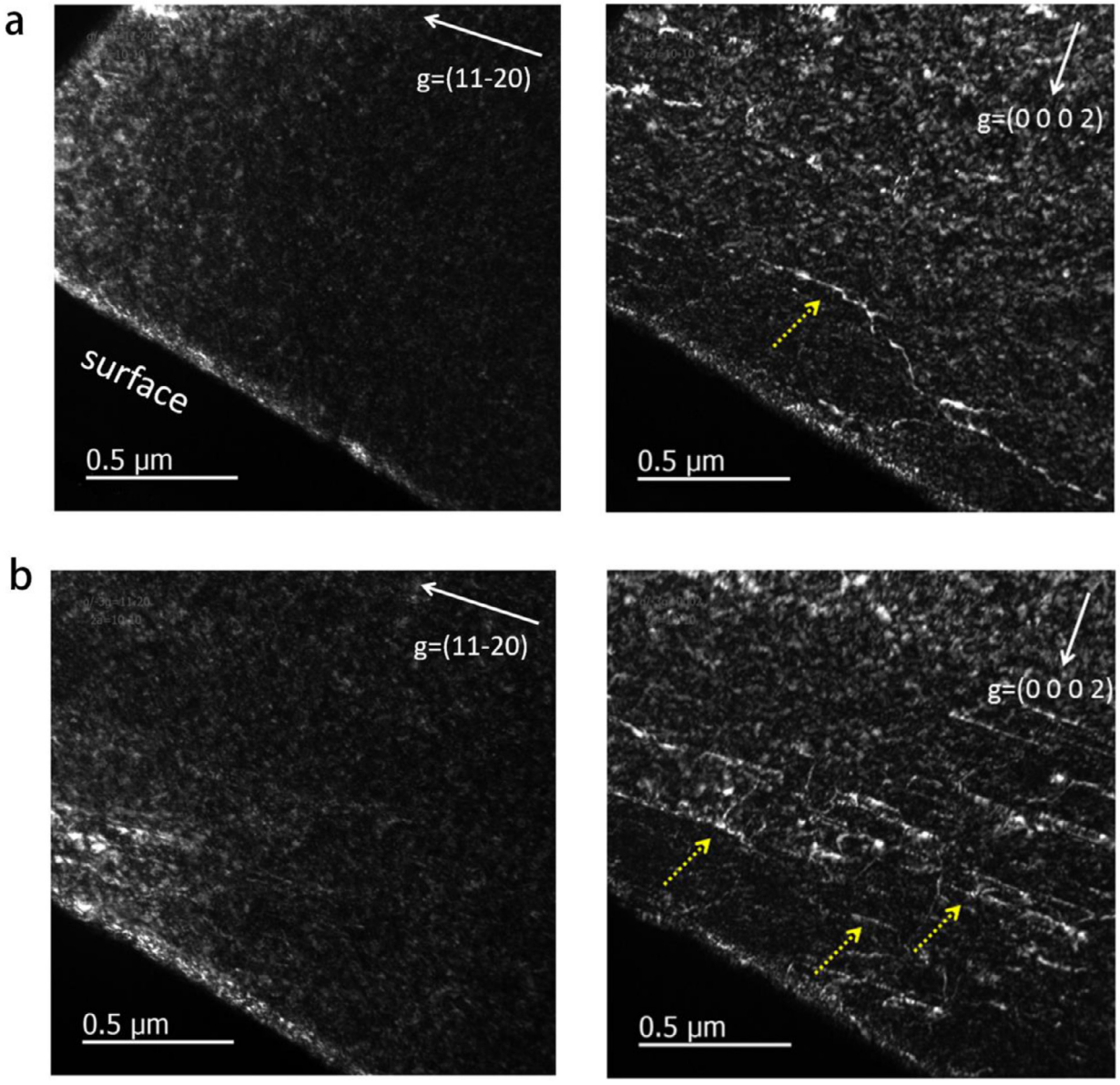

Fig. 5. **TEM dark field images of the lamella prepared by FIB-milling and lift-out.** (**a**) DF images of one region taken at **g**=(11$\bar{2}$0) and **g**=(0002), respectively. Based on the visibility criteria, almost all dislocations are <c> dislocations (marked by yellow arrows). (**b**) <c> dislocations are observed in another area of this lamellae.

line scans contain straight, near vertical bands with distinct colors. They are identified as the subsurface morphology of those prismatic slip bands observed on the surface. Based on the plane trace analysis both on the surface and on the viewing plane of Fig. 3c, the slip bands are exactly parallel to the ($\bar{1}$100) prismatic plane of Grain 1 in the 3D space.

In deformed materials, Laue diffraction peaks are often streaked due to the presence of geometrically necessary dislocations (GNDs) locally. Peak streak direction is dependent on the GND content. In particular, a set of edge GNDs having Burgers vector **b** and slip plane normal **n** would cause a diffraction peak (hkl) to be streaked in the reciprocal space along the direction of $\xi = \frac{\tau \times g_{hkl}}{|\tau \times g_{hkl}|}$ [35]. Here, g_{hkl} is the reciprocal lattice vector of peak (hkl) and $\boldsymbol{\tau}$ is the dislocation line direction ($\boldsymbol{\tau}$=**b**×**n**).

Using this theory, Laue diffraction patterns of individual voxels were examined to infer local dislocation activities. According to the beam size and our scan strategy, each voxel corresponds to a material volume of 0.5μm × 2μm × 2μm. In some voxels, diffraction peaks are sharp spots, suggesting the absence of GNDs. In other voxels particularly near the prismatic slip bands, peak streaking is observed, suggesting the presence of GNDs locally. Fig. 4a shows the Laue diffraction pattern of a voxel in line scan 2, marked by a small square in Fig. 3c. Using peak streak analysis [36,37], the slip system of those GNDs can be inferred. Fig. 4b shows the

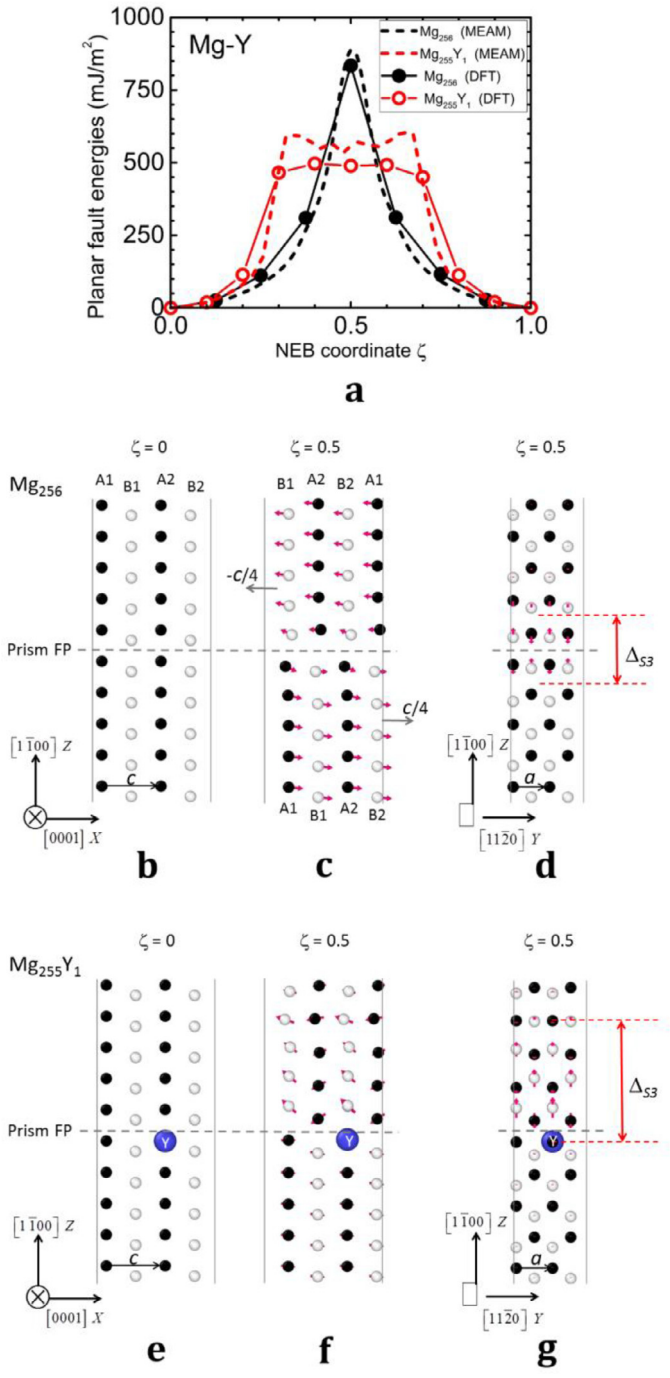

Fig. 6. **Computational study of the effect of Y solute atoms on prismatic <c> slip in Mg.** (**a**) GSFE curves along <c> direction on prismatic plane in Mg_{256} and $Mg_{255}Y_1$ according to DFT and MEAM calculations. (**b–d**) Atomic displacement and shuffle associated with a <c> dislocation in pure Mg. (**e–g**) Atomic displacement and shuffle associated with a <c> dislocation in $Mg_{255}Y_1$.

calculated peak streak direction assuming edge dislocations on fifteen different slip systems: basal <a> slip (#1−3), prismatic <a> slip (#4−6), pyramidal II <c+a> slip (#7−12), and prismatic <c> slip (#13−15). While none of the twelve regular slip systems (#1−12) can provide a good match between the calculated and the actual peak streak directions, a less common slip system $(\bar{1}100)[0001]$ (#15) gives a very close match. Note its slip plane $(\bar{1}100)$ is same as that identified for the slip bands. The μ-Laue experiment thus suggests that near the prismatic slip bands of Grain 1, there are pure <c> dislocations.

3.3. TEM characterization of <c> dislocations

To further verify that the dislocations associated with the prismatic slip bands in Grain 1 are of <c> type, we performed TEM characterizations. A thin foil crossing one of the prismatic slip bands was extracted by FIB-milling and lift-out. Its location is indicated by the blue arrow in Fig. 3a. The dimension of the foil is 15 μm (surface length) × 10 μm (depth beneath the surface). The sample was then sent to TEM for double tilt characterizations. The zone axis is $[\bar{1}100]$. The (0001) basal plane is edge-on under such observing direction. TEM dark field images were taken under two-beam condition using **g** vectors of (0002) or $(11\bar{2}0)$. As shown in Fig. 5, the dislocations are visible when **g**=(0002) but almost invisible when **g**=$(11\bar{2}0)$. Based on the invisibility criteria for dislocations (*i.e.* $\mathbf{g}\cdot\mathbf{b}=\mathbf{0}$), almost all dislocations in the view are of the <c> type. Many segments of the dislocations are nearly perpendicular to the [0002] direction, suggesting they are of edge type, while other segments are of screw or mixed type. The TEM result and the μ-Laue result together indicate that the slip bands in Grain 1 were caused by <c> dislocations on prismatic plane $(\bar{1}100)$.

4. Discussion

To the authors' knowledge, it is the first time that long-range prismatic <c> slip has been reported in a Mg alloy. The conventional wisdom is that the energy associated with <c> slip is so high that it is prohibited to independently nucleate from the matrix. Assuming that the stress state in Grain 1 was similar to the uniaxial tension applied on the specimen, the Schmid factor for $(\bar{1}100)[0001]$ slip (=0.22) was close to the Schmid factor for basal slip (=0.21), which suggests that the prismatic <c> slip is relatively easy to be activated in this material. Apparently, solute Y plays an important role for its activation.

A few computation studies have found that solute Y can critically reduce the CRSS ratio between non-basal slip and basal slip in Mg. By simulating the interaction between solute Y with dislocation cores, Kim et al. [17] estimated the ratio of $CRSS_{\text{pyramidal <c+a>}}/CRSS_{\text{basal}}$ to be reduced from a value greater than 100 in pure Mg to around 1.8 in Mg-1.0at%Y (equivalent to Mg-3.6 wt%Y). Another study by Tsuru and Chrzan [20] using DFT estimated the ratio of $CRSS_{\text{prism <a>}}/CRSS_{\text{basal}}$ to be reduced from a value greater than 20 in pure Mg to around 1.5 in Mg-1.0at%Y.

So far, the influence of Y solute on <c> slip has not been computationally studied, mostly because <c> slip has rarely been observed in Mg or any other hexagonal metals. To understand this issue, we calculated the generalized stacking fault energy (GSFE) curve along <c> direction

on prismatic plane using a supercell of 256 Mg atoms (Mg_{256}) and re-calculated it by replacing one Mg atom with one Y atom ($Mg_{255}Y_1$). The supercell was adopted to produce a c-fault over a faulting area 2a×2c, where a=3.20 Å, c = 5.19 Å (c/a ratio ~1.622), with 64 atomic layers in the perpendicular direction and a pair of free surfaces. The calculation was performed using both DFT and MD with modified embedded atom methods (MEAM) potential developed by Kim et al. [38]. The DFT calculation was performed with Vienna Ab initio Simulation Package (VASP) [39], using a plane-wave basis with the projector-augmented wave (PAW) method [40] and potentials generated by Kresse and Joubert [41]. The electronic exchange and correlation effects are described by a generalized gradient approximation [42], and a plane-wave energy cutoff of 385 eV. The GSFE curves were obtained with nudged elastic band (NEB) techniques [43], following a similar calculation procedure described in an earlier study of basal GSFEs in Mg [44]. In terms of planar stacking fault energy, the two sets of NEB calculations yield similar values for Mg, *i.e.*, 0.834 J/m^2 (DFT) and 0.927 J/m^2 (MEAM), as shown in Fig. 6a. These values are consistent with the similar calculation results in [24], and they are much higher than that of a planar <a> fault on the basal plane (0.09–0.13 J/m^2) [38, 44]. When a <c> dislocation is generated on the prismatic plane (Fig. 6b−d), atomic shuffle along the prismatic plane normal direction (prismatic shuffle, Δ_{S3}) is necessary. If one Mg atom right below the prismatic fault plane is replaced by a solute atom Y (Fig. 6e and f), the magnitude of prismatic shuffle is increased such that atomic relaxations extend strongly over a distance of about 10 Å ($\Delta_{S3} \sim 2\sqrt{3}a$) above the fault plane (Fig. 6g). The consequence is so significant that the energy barriers for the <c> fault can be reduced by almost 40% according to both DFT and MEAM calculations (Fig. 6a). This calculation indicates that solute Y can lower the energy barrier for <c> dislocation to nucleate in Mg lattice.

Activation of <c> slip increases the number of independent slip systems that can accommodate the external strain. This can explain the enhanced ductility of Mg-Y compared with pure Mg. When free <c> dislocations encountered <a> dislocations in the same grain, they might jointly form $\{10\bar{1}2\}$ twin embryos through the classic "pole mechanism" [45] that does not require twinning dislocations on the $\{10\bar{1}2\}$ plane. Ghazisaeidi and Curtin suggested that a <c> dislocation in Mg can dissociate and assist the formation of a 6-layer-thick $\{10\bar{1}2\}$ twin embryo [46]. Under the above mechanisms, twin nucleation does not necessarily abide by the Schmid law. The presence of <c> dislocations can potentially explain the twin nucleation in Grain 1 even when the Schmid factor for twinning was negative (Fig. 3b). Nevertheless, those twins lacked the driving force for their further growth due to the negative shear stress.

5. Conclusions

In summary, the Mg-2.5wt%Y cast alloy shows excellent tensile ductility. From an *in situ* tensile test, long-range prismatic slip bands developed during deformation. μ-Laue and TEM characterization revealed that these slip bands were associated with the unusual <c> dislocations. Nucleation of <c> dislocations is attributed to Y solute atoms reducing the stacking fault energy along <c> direction on prismatic planes. Activity of <c> dislocations likely contributes to the high ductility of this Mg-2.5wt%Y alloy. <c> dislocations in the Mg lattice could assist the nucleation of $\{10\bar{1}2\}$ twin embryos, even if the Schmid factor for twinning was negative.

Acknowledgments

We thank Prof. Erica Lilleodden and Dr. Julian Sabisch for the initial discussion. This work has been financially supported by the National Natural Science Foundation of China (Nos. 51671127, 51631006, 51971168). L.W. is sponsored by the Shanghai Rising-Star Program. Use of the Advanced Photon Source was supported by the United States Department of Energy, Office of Science, Office of Basic Energy Sciences, under Contract No. DE-AC02–06CH11357.

References

[1] J.F. Nie, K.S. Shin, Z.R. Zeng, Metall. Mater. Trans. A 51 (2020) 6045–6109, doi:10.1007/s11661-020-05974-z.
[2] J.H. Hwang, A. Zargaran, G. Park, O. Lee, B.J. Lee, N.J. Kim, J. Magnes. Alloy. 9 (2021) 489–498, doi:10.1016/j.jma.2020.09.016.
[3] C.M. Byer, B. Li, B. Cao, K.T. Ramesh, Scr. Mater. 62 (2010) 536–539, doi:10.1016/j.scriptamat.2009.12.017.
[4] S. Nandy, S.P. Tsai, L. Stephenson, D. Raabe, S. Zaefferer, J. Magnes. Alloy. 9 (2021) 1521–1536, doi:10.1016/j.jma.2021.03.005.
[5] K.Y. Xie, Z. Alam, A. Caffee, K.J. Hemker, Scr. Mater. 112 (2016) 75–78, doi:10.1016/j.scriptamat.2015.09.016.
[6] B.Y. Liu, F. Liu, N. Yang, X.B. Zhai, L. Zhang, Y. Yang, B. Li, J. Li, E. Ma, J.F. Nie, Z.W. Shan, Science 365 (2019) 73–75, doi:10.1126/science.aaw2843.
[7] Q. Yu, L. Qi, R.K. Mishra, J. Li, A.M. Minor, Proc. Natl. Acad. Sci. USA 110 (2013) 13289–13293, doi:10.1073/pnas.1306371110.
[8] R. Ahmad, B. Yin, Z. Wu, W.A. Curtin, Acta Mater. 172 (2019) 161–184, doi:10.1016/j.actamat.2019.04.019.
[9] S. Sandlöbes, S. Zaefferer, I. Schestakow, S. Yi, R. Gonzalez-Martinez, Acta Mater. 59 (2011) 429–439, doi:10.1016/j.actamat.2010.08.031.
[10] W. Li, L. Wang, B. Zhou, C. Liu, X. Zeng, J. Mater. Sci. Technol. 35 (2019) 2200–2206, doi:10.1016/j.jmst.2019.04.030.
[11] A. Maldar, L. Wang, G. Zhu, X. Zeng, J. Magnes. Alloy. 8 (2020) 210–218, doi:10.1016/j.jma.2019.07.009.
[12] D.D. Yin, C.J. Boehlert, L.J. Long, G.H. Huang, H. Zhou, J. Zheng, Q.D. Wang, Int. J. Plast. 136 (2021) 102878, doi:10.1016/j.ijplas.2020.102878.
[13] G. Wu, C. Wang, M. Sun, W. Ding, J. Magnes. Alloy. 9 (2021) 1–20, doi:10.1016/j.jma.2020.06.021.
[14] J. Wang, G. Zhu, L. Wang, Q. Zhu, E. Vasilev, X. Zeng, M. Knezevic, Materialia 15 (2021) 101038, doi:10.1016/j.mtla.2021.101038.
[15] S. Sandlöbes, Z. Pei, M. Friák, L.F. Zhu, F. Wang, S. Zaefferer, D. Raabe, J. Neugebauer, Acta Mater. 70 (2014) 92–104, doi:10.1016/j.actamat.2014.02.011.
[16] Z. Ding, W. Liu, H. Sun, S. Li, D. Zhang, Y. Zhao, E.J. Lavernia, Y. Zhu, Acta Mater. 146 (2018) 265–272, doi:10.1016/j.actamat.2017.12.049.
[17] K.H. Kim, J.B. Jeon, N.J. Kim, B.J. Lee, Scr. Mater. 108 (2015) 104–108, doi:10.1016/j.scriptamat.2015.06.028.
[18] Z. Wu, R. Ahmad, B. Yin, S. Sandlöbes, W.A. Curtin, Science 359 (2018) 447–452, doi:10.1126/science.aap8716.
[19] J.A. Yasi, L.G. Hector Jr, D.R. Trinkle, Acta Mater. 59 (2011) 5652–5660, doi:10.1016/j.actamat.2011.05.040.

[20] T. Tsuru, D.C. Chrzan, Sci. Rep. 5 (2015) 8793, doi:10.1038/srep08793.
[21] Z. Huang, L. Wang, Z. Zhou, T. Fischer, S. Yi, X. Zeng, Scr. Mater. 143 (2018) 44–48, doi:10.1016/j.scriptamat.2017.09.011.
[22] D. Zhang, L. Jiang, X. Wang, I.J. Beyerlein, A.M. Minor, J.M. Schoenung, S. Mahajan, E.J. Lavernia, J. Mater. Res. 34 (2019) 1542–1554, doi:10.1557/jmr.2019.124.
[23] N. Stanford, R.K.W. Marceau, M.R. Barnett, Acta Mater. 82 (2015) 447–456, doi:10.1016/j.actamat.2014.09.022.
[24] H. Fan, J. Tang, X. Tian, Q. Wang, X. Tian, J.A. El-Awady, Scr. Mater. 135 (2017) 37–40, doi:10.1016/j.scriptamat.2017.03.012.
[25] M. Ghazisaeidi, L.G. Hector, W.A. Curtin, Scr. Mater. 75 (2014) 42–45, doi:10.1016/j.scriptamat.2013.11.013.
[26] D. Zhang, L. Jiang, J.M. Schoenung, S. Mahajan, E.J. Lavernia, Philos. Mag. 95 (2015) 3823–3844, doi:10.1080/14786435.2015.1100764.
[27] Z.X. Wu, W.A. Curtin, Nature 526 (2015) 62–67, doi:10.1038/nature15364.
[28] K. Wei, L. Xiao, B. Gao, L. Li, Y. Liu, Z. Ding, W. Liu, H. Zhou, Y. Zhao, J. Magnes. Alloy. 8 (2020) 1221–1227, doi:10.1016/j.jma.2019.09.015.
[29] K. Wei, R. Hu, D. Yin, L. Xiao, S. Pang, Y. Cao, H. Zhou, Y. Zhao, Y. Zhu, Acta Mater. 206 (2021) 116604, doi:10.1016/j.actamat.2020.116604.
[30] W. Xu, Y. Zhang, G. Cheng, S.N. Mathaudhu, R.O. Scattergood, C.C. Koch, E.J. Lavernia, Y. Zhu, Acta Mater. 131 (2017) 457–466, doi:10.1016/j.actamat.2017.04.015.
[31] G. Zhu, L. Wang, H. Zhou, J. Wang, Y. Shen, P. Tu, H. Zhu, W. Liu, P. Jin, X. Zeng, Int. J. Plast. 120 (2019) 164–179, doi:10.1016/j.ijplas.2019.04.020.
[32] B.C. Larson, W. Yang, G.E. Ice, J.D. Budai, J.Z. Tischler, Nature 415 (2002) 887–890, doi:10.1038/415887a.
[33] G.E. Ice, J.D. Budai, J.W.L. Pang, Science 334 (2011) 1234–1239, doi:10.1126/science.1202366.
[34] D. Zhang, H. Wen, M.A. Kumar, F. Chen, L. Zhang, I.J. Beyerlein, J.M. Schoenung, S. Mahajan, E.J. Lavernia, Acta Mater. 120 (2016) 75–85, doi:10.1016/j.actamat.2016.08.037.
[35] R.I. Barabash, G.E. Ice, F.J. Walker, J. Appl. Phys. 93 (2003) 1457–1464, doi:10.1063/1.1534378.
[36] L. Wang, M. Li, J. Almer, T. Bieler, R. Barabash, Front. Mater. Sci. 7 (2013) 156–169, doi:10.1007/s11706-013-0201-0.
[37] B. Zhou, L. Wang, W. Liu, J. Wang, X. Zeng, W. Ding, Mater. Charact. 156 (2019) 109873, doi:10.1016/j.matchar.2019.109873.
[38] K.H. Kim, J.B. Jeon, B.J. Lee, Calphad 48 (2015) 27–34, doi:10.1016/j.calphad.2014.10.001.
[39] G. Kresse, J. Furthmuller, Phys. Rev. B 54 (1996) 11169–11186, doi:10.1103/PhysRevB.54.11169.
[40] P.E. Blöchl, Phys. Rev. B 50 (1994) 17953–17979, doi:10.1103/PhysRevB.50.17953.
[41] G. Kresse, D. Joubert, , Phys. Rev. B 59 (1999) 1758–1775. 10.1103/PhysRevB.59.1758.
[42] J.P. Perdew, Y. Wang, Phys. Rev. B 45 (1992) 13244–13249, doi:10.1103/PhysRevB.45.13244.
[43] G. Henkelman, H. Jónsson, J. Chem. Phys. 113 (2000) 9978–9985, doi:10.1063/1.1323224.
[44] Q. Dong, Z. Luo, H. Zhu, L. Wang, T. Ying, Z. Jin, D. Li, W. Ding, X. Zeng, J. Mater. Sci. Technol. 34 (2018) 1773–1780, doi:10.1016/j.jmst.2018.02.009.
[45] J.W. Christian, S. Mahajan, Prog. Mater. Sci. 39 (1995) 1–157, doi:10.1016/0079-6425(94)00007-7.
[46] M. Ghazisaeidi, W.A. Curtin, Model. Simul. Mater. Sci. Eng. 21 (2013) 055007, doi:10.1088/0965-0393/21/5/055007.